Dual [proton]/[hole] mixed valence in a molecular metal: balancing chemical activity in the solid state by tapping into a molecular hole reservoir†

Youssef Lakhdar,[a] Cécile Mézière,[a] Leokadiya Zorina,[ab] Michel Giffard,[a] Patrick Batail,*[a] Enric Canadell,*[c] Pascale Auban-Senzier,[d] Claude Pasquier,[d] Denis Jérome,[d] Bálint Náfrádi[e] and László Fórró[e]

Received 1st September 2010, Accepted 8th November 2010
DOI: 10.1039/c0jm02897e

We report on the synthesis, the layered triclinic $P\bar{1}$ crystal structure, band structure and Fermi surface analysis and preliminary transport and ESR data of β-(EDT-TTF-I_2)$_2^{(1+x)\bullet+}$[HO_2C–CH=CH–CO_2^-]$_{(1-x)}$[^-O_2C–CH=CH–CO_2^-]$_x$, a metallic radical cation salt of the nominal, mono-deprotonated π-conjugated dicarboxylate anion of fumaric acid with a metal–insulator transition at *ca.* 70 K and conclude that the system is doped, that is, a fraction of the fumarates are further deprotonated to their dianion forms. It is shown that the actual number of protons required within the extended fumarate network to effectively balance the chemical activity at the nuclei/solution interface during crystal growth is compensated by tapping into the HOMO bands serving as a molecular hole reservoir such that the compound formulation and structure remain intact. A dual [proton]/[hole] mixed-valence is thereby revealed and defined as the duality between the modulation of the electrostatic potential of the environment, the incommensurate number and the physics of migrating holes within a molecular system.

Introduction

The opportunity to balance and get control of the electrostatics of molecular systems based on conjugated carboxylates has been developed in recent years and is still growing in scope in the fields of organic conductors,[1,2] and organic electrodes for batteries.[3] In the wake of earlier work using interfacial C–$I_{organic}$···$I_{inorganic}$ halogen bonding interactions to direct the structure of organic and hybrid metals,[4] the present research was designed to explore the outcome of competing hydrogen and halogen-bonding interactions in directing the topology and electronic structure of radical cation salts of organic polycarboxylates.[1,2] This turned out, as exemplified herein, to address fundamental issues associated with balancing the proton activity [H^+] at organic–organic interfaces during crystal growth[5] by tapping off the upper HOMO band of the conducting slab serving as a molecular hole reservoir whose outcome is the installation of an irrational net electron count. A [proton]/[hole] mixed-valence phenomenon[6] is thereby revealed and defined in this paper as the duality between the modulation of the electrostatic potential of the environment, the incommensurate number, and subsequent physics of migrating holes in the conducting slabs of β-(EDT-TTF-I_2)$_2^{\bullet+}$[HO_2C–CH=CH–CO_2^-], a metallic radical cation salt of the mono-deprotonated π-conjugated dicarboxylate anion of fumaric acid. Hence, the dual [proton]/[hole] mixed-valence state discussed in this paper is seen as the inherent expression during crystal nucleation and growth[5] of a thermodynamic equilibrium where the number of protons and holes stabilized upon balancing the chemical potential at kT need not to be an integer, providing a molecular hole reservoir, here the HOMO band based, made available so that the net number of molecules and structure of the system remain intact.

Experimental

Electrocrystallization

A two-compartment cell equipped with platinum electrodes (l = 2 cm, $Ø$ = 1 mm) and kept at 30 °C was filled with a dichloromethane (11 mL, dried over N alumina) solution and a methanol (1 mL, distilled over CaH_2) solution containing ethylenedithio-1,2-diiodo-tetrathiafulvalene, EDT-TTF-I_2 (5 mg) (Scheme 1), twice crystallized in toluene,[7] and Bu_4N[HO_2C–CH=CH–CO_2^-][1e] (100 mg) which serves as an electrolyte. Oxidation at low constant current (0.5 μA) afforded high quality, large plate-like single crystals such as the one in Fig. 1 after 10 days.

X-Ray structure analysis

Crystal data: $C_{20}H_{11}I_4O_4S_{12}$, M = 1207.61, triclinic, $P\bar{1}$, a = 8.1576(4), b = 13.170(1), c = 15.4841(9) Å, α = 78.710(7),

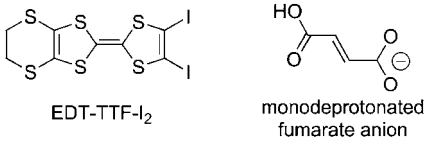

Scheme 1 Molecular structures of the two components.

[a]*Institut des Sciences et Technologies Moléculaires, Université d'Angers, CNRS, UMR 6200 MOLTECH, 49045 Angers, France. E-mail: patrick.batail@univ-angers.fr*
[b]*Institute of Solid State Physics RAS, 142432 Chernogolovka, MD, Russia*
[c]*Institut de Ciència de Materials de Barcelona (ICMAB-CSIC), Campus de la UAB, E-08193 Bellaterra, Spain. E-mail: canadell@icmab.es*
[d]*Laboratoire de Physique des Solides, Université de Paris-Sud, CNRS, UMR, 91405 Orsay, France*
[e]*Institut de Physique de la Matière Complexe, Ecole Polytechnique Fédérale de Lausanne (EPFL), 1015 Lausanne, Switzerland*
† CCDC reference number 790256. For crystallographic data in CIF or other electronic format see DOI: 10.1039/c0jm02897e

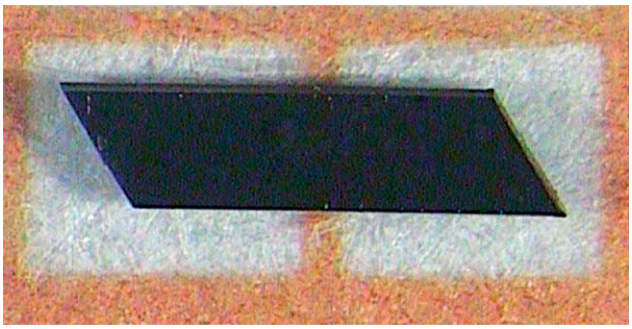

Fig. 1 A 2 mm long single crystal of β-(EDT-TTF-I_2)$_2$[HO_2C–CH=CH–CO_2] grown by electrocrystallization.

b = 80.782(5), γ = 88.271(6)°, V = 1610.3(2) Å^3, Z = 2, D_{calc} = 2.491 g cm^{-3}, μ = 46.79 cm^{-1}, F(000) = 1134, T = 293(2) K, $2\theta_{max}$ = 60°, reflections measured 49 416, unique reflections 9373 (R_{int} = 0.0373), reflections with $I > 2\sigma(I)$ = 6388, parameters refined 361, R_1 = 0.0270, wR_2 = 0.0489, GOF = 1.008.

X-Ray data were collected at room temperature on a single crystal using a Bruker Nonius KappaCCD diffractometer with monochromatized MoK_α-radiation (λ = 0.71073 Å, graphite monochromator, combined φ/ω-scan). Empirical absorption correction of experimental intensities was applied using the SADABS program.[8] The structure was solved by a direct method followed by Fourier syntheses and refined by a full-matrix least-squares method in an anisotropic approximation for all non-hydrogen atoms using the SHELX-97 programs.[9] H-atoms were placed in idealized positions and refined using a riding model with U_{iso}(H) fixed at 1.2U_{eq}(C) and 1.5U_{eq}(O).†

Transport measurements

Resistivity measurements were conducted on single crystals for both in-plane and transverse (perpendicular to the plane) configurations in order to get $\rho_{||}$ and $\rho_{\perp}$. Gold evaporations were performed in order to improve the geometry and the quality of the contacts. Four aligned contacts were made on both sides of the platelets for in-plane resistivity measurements and two contacts on each side of the platelets for transverse resistivity measurements. Samples were cooled down to 25 K using a cryocooler. A low frequency lock-in technique was used with low ac currents, 10 μA for $\rho_{||}$ and 1 μA for $\rho_{\perp}$. When the current is injected into the plane, a large unnested voltage is measured (of the same order of the voltage associated to the normal resistance) which indicates ill-defined current lines and prevents from an accurate determination of the in-plane resistivity. Hence, the resistance ($R_{||}$) is plotted in Fig. 4 instead of the resistivity.

Electronic structure

The tight-binding band structure calculations were of the extended Hückel type.[10] A modified Wolfsberg–Helmholtz formula was used to calculate the non-diagonal $H_{\mu\nu}$ values.[11] All valence electrons were taken into account in the calculations and the basis set consisted of Slater-type orbitals of double-ζ quality for C 2s and 2p, S 3s and 3p and of single-ζ quality for H. The ionization potentials, contraction coefficients and exponents were taken from previous work.[12]

Spin susceptibility

Electron spin resonance measurements were performed on a single crystal with a commercial Bruker ELEXSYS E500 spectrometer at 9.4 GHz excitation frequency. The temperature was controlled in the 4–300 K range with an Oxford ESR900 cryostat.

Results and discussion

Our primary intention was to try and provoke the deliberate association in the solid state (Fig. 1) of collections of two constituents (Scheme 1), namely, the radical cation EDT-TTF-$I_2^{\bullet+}$ and the fumarate anion [HO_2C–CH=CH–CO_2^-]. Here, C–I···O halogen bonds and one O–H···O hydrogen bond (Fig. 2a), and weak C_{sp^3}–H···O hydrogen bonds, competing with p_π–p_π overlap interactions between the redox cores, are expected and indeed exacted at the organic–organic interface, yielding the

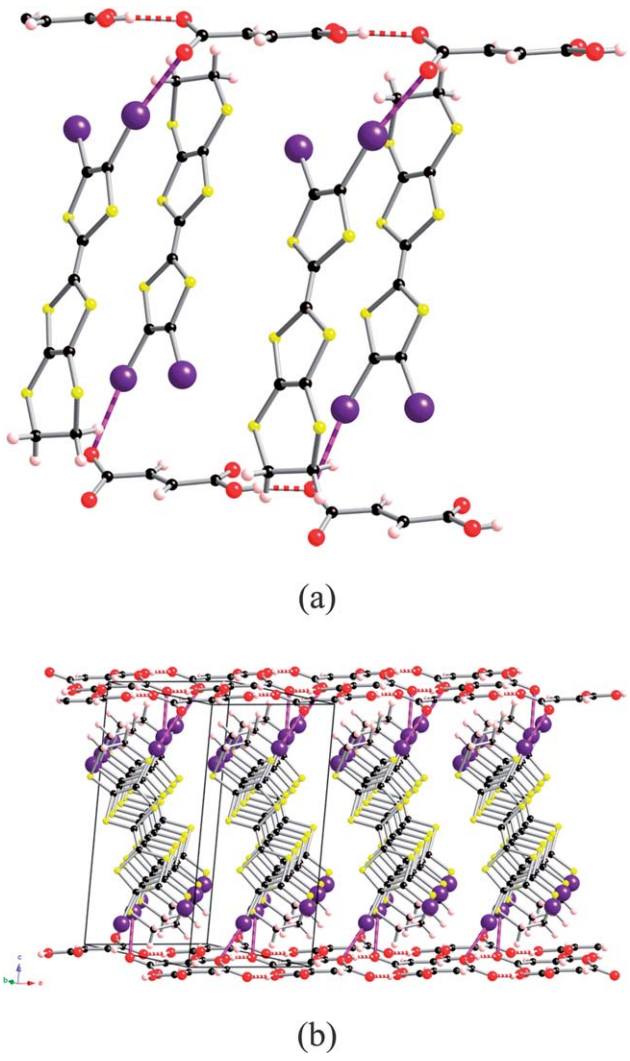

Fig. 2 (a) Two C–I···O halogen bonds (2.736(2) and 2.896(2) Å) at the organic–organic interface and one O–H···O hydrogen bond (1.81 Å) between the fumarate anions (discussed further in Fig. 3) are identified in β-(EDT-TTF-I_2)$_2^{\bullet+}$[HO_2C–CH=CH–CO_2^-]. The balance of these intermolecular interactions and p_π–p_π overlap interactions between the π-conjugated radical cation cores yields a layered structure (b).

layered all-organic metal, β-(EDT-TTF-I_2)$_2^{\bullet+}$[HO_2C–CH=CH–CO_2^-] where three such interactions are satisfied, as exemplified in Fig. 2b. Note also that, from the viewpoint of the dense, two-dimensional pattern of association of the fumaric acid units in the solid state[13] shown in Fig. 3b, the fumarate anions are farther apart in the direction transverse to the O–H···O hydrogen bonded strings in β-(EDT-TTF-I_2)$_2$[HO_2C–CH=CH–CO_2] (Fig. 3a).

The asymmetric unit of the triclinic $P\bar{1}$ lattice contains two independent EDT-TTF-I_2 π-donor molecules and one fumarate anion, both in general positions. The structure refinement leaves no ambiguity as to which is the carboxylic acid or carboxylate end group location in the latter as the proton is unambiguously assigned to the neutral –COOH group with C=O and C–O(H) bonds equal to 1.199(3) and 1.320(3) Å, respectively. Conversely, the negative charge of $–COO^-$ ion is shared between both oxygen atoms, smoothing out the difference in their C–O bond lengths to 1.246(3) and 1.265(3) Å. Note also that the inner C=C bond lengths in the TTF cores of EDT-TTF-I_2 are practically identical at 1.363(3) and 1.361(3) Å. The β-type conducting layer topology is described further in the section concerning the HOMO···HOMO interactions.

Metallic character for both the in-plane resistance, $\rho_{\parallel}$, and the transverse resistivity, $\rho_{\perp}$

Both in-plane resistance and transverse resistivity of β-(EDT-TTF-I_2)$_2$[HO_2C–CH=CH–CO_2] show metallic behaviour down to 70–80 K where the system becomes localized (Fig. 4). At room temperature, the transverse resistivity amounts to 50 Ω cm and the in-plane resistivity would be 10 mΩ cm providing the unnested voltage was not taken into account.

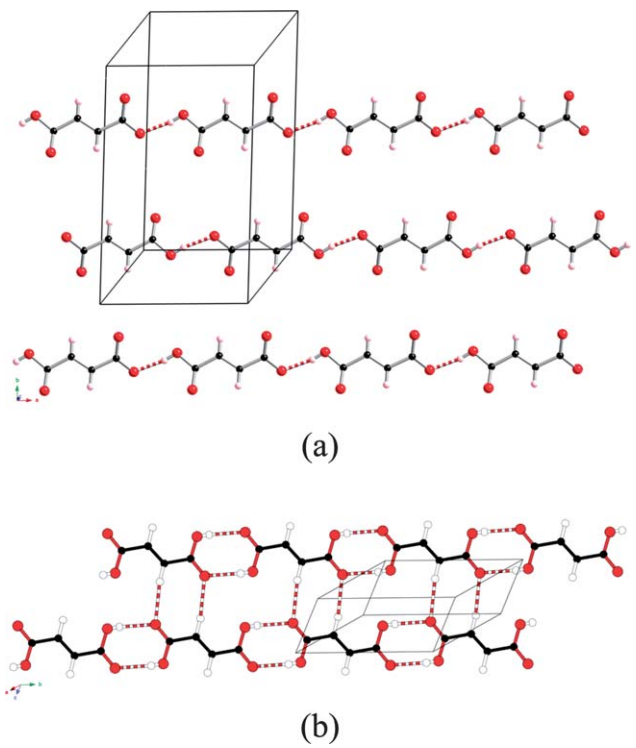

Fig. 3 (a) The hydrogen bonded strings of fumarate anions are farther apart in the lattice in β-(EDT-TTF-I_2)$_2$[HO_2C–CH=CH–CO_2], spread out so as to answer the demand of the C–I···O halogen bonds, thereby preventing the formation of the transverse C–H···O, 2.38 Å, hydrogen bonds which, in addition to classical carboxylic acid O–H···O, 2.00 Å hydrogen bond dimers, stabilize the two-dimensional lattice in HO_2C–CH=CH–CO_2H, the pure acid crystal form is shown in (b).

Nature of the HOMO···HOMO interactions

As shown in Fig. 5 the repeat unit of the donor layers in β-(EDT-TTF-I_2)$_2$[HO_2C–CH=CH–CO_2] contains four donors of two different types (A and B) which make stacks of the ···A–A–B–B–A–A··· type. The donor layers are built from such parallel stacks running along the (a + b) direction. There are three different types of donor···donor interactions within the stacks (noted I to III in Fig. 5) and five different types of donor···donor interactions between the stacks (noted IV to VIII in Fig. 5). To analyze the relationship between the crystal and band structures of this system we have evaluated the strength of the eight different HOMO···HOMO interaction energies[14] (β) in the donor layers. The calculated $|\beta_{HOMO–HOMO}|$ values are reported in Table 1.

The central C=C bond lengths for A and B are very similar and, as expected, the HOMO energies of the two donors are very close ($\Delta \approx 0.02$ eV). The three intrastack interactions are remarkably similar and quite strong. The similarity in both HOMO energies and strength of the intrastack interactions as well as in interplanar separations between adjacent radical cations along the stack (3.51(2), 3.52(2) and 3.53(1) Å for I, II and III, respectively) qualifies the stacks along (a + b) as almost uniform, as far as the HOMO···HOMO interactions are concerned, despite the fact that structurally they are not. Although non-negligible, the five interstack interactions are one order of magnitude weaker. Note, however, that there are eight of them per repeat unit so that the effective interstacks interaction is smaller than the intrastack ones but quite sizeable. Consequently, as far as the HOMO···HOMO interactions (*i.e.*, those determining the transport properties of the system) are concerned, these layers should be described as a series of interacting almost uniform chains along the (a + b) direction.

A molecular hole reservoir

The calculated band structure near the Fermi level is shown in Fig. 6. Since the repeat unit contains four donors, this band

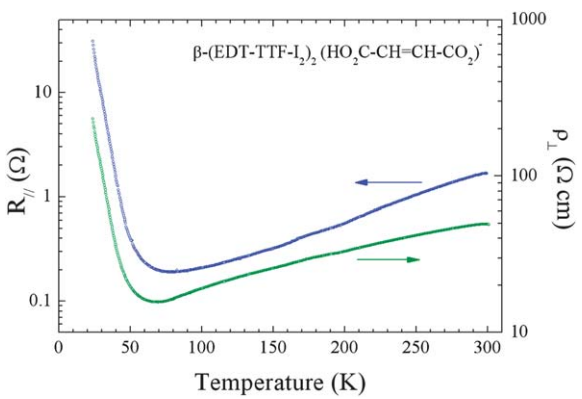

Fig. 4 Temperature dependence of the in-plane resistance ($R_{\parallel}$, left scale) and transverse resistivity ($\rho_{\perp}$, right scale) of β-(EDT-TTF-I_2)$_2$[HO_2C–CH=CH–CO_2] at ambient pressure.

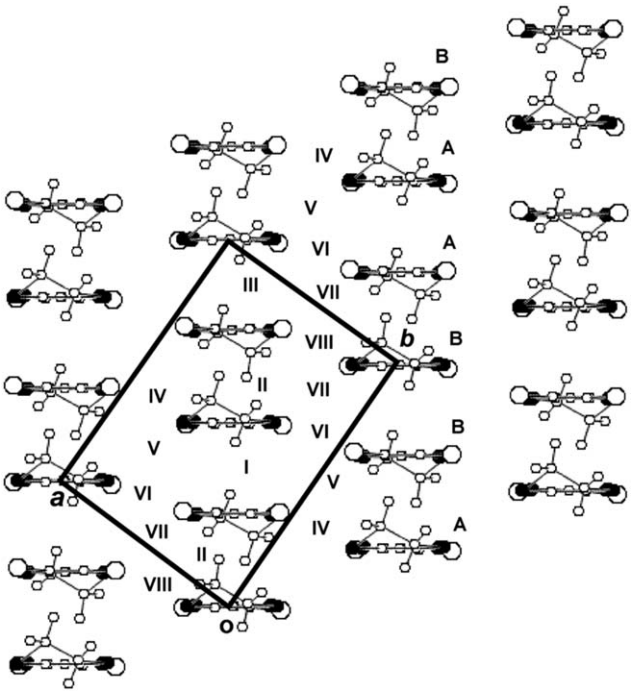

Fig. 5 Donor layer in β-(EDT-TTF-I_2)$_2$[HO_2C–CH=CH–CO_2] where the different types of donor···donor interactions are labeled and whose calculated values are available in Table 1.

Table 1 Calculated values of the $|\beta_{HOMO-HOMO}|$ (eV) for the different donor···donor interactions in the donor layers of β-(EDT-TTF-I_2)$_2$[HO_2C–CH=CH–CO_2]

Interaction (type)	$\|\beta_{HOMO-HOMO}\|$
I (A–A)	0.4015
II (A–B)	0.3809
III (B–B)	0.3901
IV (A–A)	0.0178
V (A–B)	0.0501
VI (A–B)	0.0320
VII (A–B)	0.0555
VIII (B–B)	0.0213

structure contains four bands almost exclusively built from the HOMOs of the four donors. Assuming the fumarate to be in its nominal, monoanionic monodeprotonated form, there should be two holes in the bands of Fig. 6. Note that the upper two bands are separated by a small band gap. We have verified that this band gap does not close inside the Brillouin zone so that the upper band should be completely empty and the system should be a small band gap semiconductor yet it is metallic (Fig. 4). The only alternative is to conclude that the system is doped instead, that is, a fraction of the fumarates are further deprotonated to their dianion forms, as schematized in Scheme 2. Hence, the novel formulation, β-(EDT-TTF-I_2)$_2^{(1+x)\bullet+}$[HO_2C–CH=CH–CO_2^-]$_{(1-x)}$[^-O_2C–CH=CH–CO_2^-]$_x$. With a fraction x of the anions being stabilized in the lattice as dianions, holes are created in the quite dispersive second highest band, that is, out of the large collection of overlapping radical cation core HOMOs in the direct space, the hole reservoir in the crystal, thereby leading to a typical metallic behavior. Hence, balancing chemical activity at

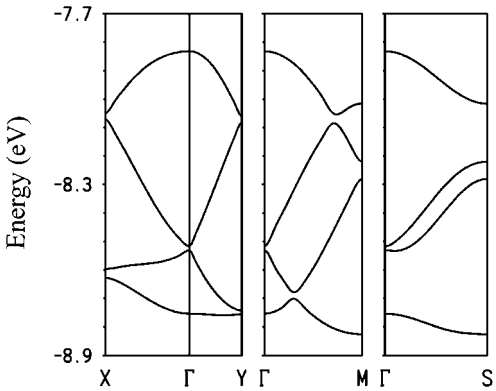

Fig. 6 Calculated band structure near the Fermi level for the donor layers of β-(EDT-TTF-I_2)$_2$[HO_2C–CH=CH–CO_2], where $\Gamma = (0, 0)$, $X = (a^*/2, 0)$, $Y = (0, b^*/2)$ $M = (a^*/2, b^*/2)$ and $S = (-a^*/2, b^*/2)$, respectively.

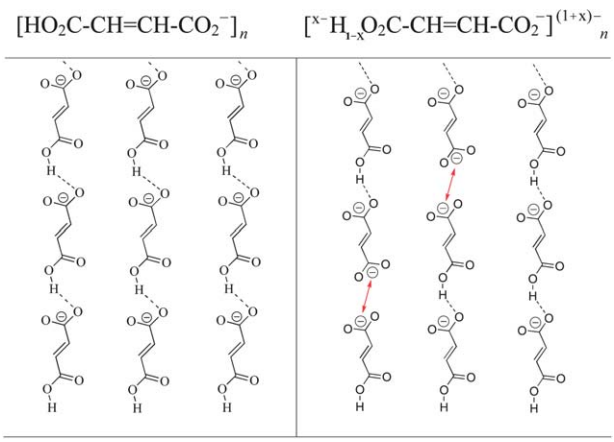

Scheme 2 Small amounts of random proton vacancies stabilised during crystal growth within the fumarate slab yield an irrational slab net negative charge.

the organic–organic interface during crystal growth[5] ultimately correlates with incommensurate band fillings, a consequence of an inherent dual [proton]/[hole] mixed valence.

Duality: the physics allows to measure the number of holes, hence *x*

Shown in Fig. 7a and b are the calculated Fermi surfaces when the Fermi level was arbitrarily lowered by 0.05 and 0.09 eV with respect to the top of the second upper band, respectively. These values correspond to an average number of extra holes of 0.097 and 0.162 per donor, *i.e.* 19.4% and 32.5% of the anions should be dianions, respectively. These Fermi surfaces are made of parallel warped lines, which are very well nested by a vector q (see Fig. 7). Therefore, a structural modulation with wave vector q would be expected to completely destroy these Fermi surfaces and the resistivity *vs.* temperature curve would exhibit a metal to insulator transition,[15] as indeed observed. Such type of behavior is kept up to Fermi level lowerings corresponding to approximately 50% of the anions being dianions. Consequently, these model calculations clearly show that for any reasonable fraction

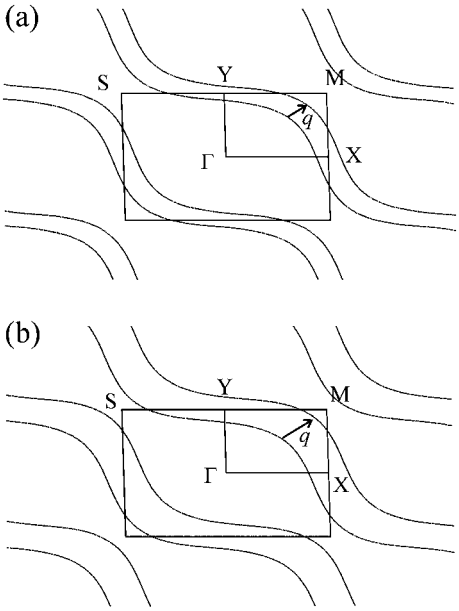

Fig. 7 Calculated Fermi surfaces for the donor layers of β-(EDT-TTF-I_2)$_2$[HO_2C–CH=CH–CO_2] when the Fermi level was lowered by 0.05 (a) and 0.09 eV (b) with respect to the top of the second upper band in Fig. 6, respectively. This corresponds to the existence of 0.097 and 0.162 additional holes per donor, respectively.

of dianions in the lattice this salt should be a pseudo-one dimensional (pseudo-1D) metal undergoing a low temperature metal to insulator transition associated with a structural modulation with q wave vector.

What is the physical meaning of these results? It may be difficult to recognize the occurrence of a pseudo-1D band in the band structure of Fig. 6 simply because the repeat vectors of the layer are both interstack vectors. However, things become simpler when realizing, as shown in Fig. 8, that the stacks of Fig. 5 run along the (a + b) diagonal direction, which coincides with the (a* + b*) diagonal direction in Fig. 8. In other words, the Fermi surface contains warped lines in a direction perpendicular to (a + b), which is the direction of the strongly interacting almost uniform stacks of HOMOs. These lines are considerably warped because, as mentioned before, the interstack interactions are weaker than the intrastack ones yet they are quite sizeable. The nesting vector q is a vector in the direction of the stacks, which is a diagonal direction. Thus, the modulation associated with the metal to insulator transition should increase the periodicity in the stacks direction. Let us note that the ratio between the length of the q vector and half the length of the diagonal in the stacks direction of the 2D primitive zone (*i.e.* $\Gamma \rightarrow M$ in Fig. 6) must be very close to the ratio between the number of dianions and the total number of anions in the lattice. Thus, future work will include an X-ray diffuse scattering study using synchrotron radiation as it would be very useful in testing our proposal concerning the conducting properties of this salt and, if the mechanism was confirmed, in giving an indication of the proportion of dianions in the lattice.

The spin susceptibility measured on a single crystal from the integrated ESR line (Fig. 9a) shows strong temperature dependence like most 1D organic conductors (*e.g.* TTF–TCNQ). In the high-temperature metallic phase the susceptibility is slowly decreasing at decreasing temperature. Below the metal–insulator transition the itinerant susceptibility falls exponentially. The good resolution of this transition in χ is precluded by about 5% of impurities, which are dominating the low temperature Curie-like ESR spectrum. Furthermore, the temperature dependence of the ESR line width (Fig. 9b) gives further insight into the dimensionality of the high temperature Q1D metallic phase although it is also complicated due to impurities similarly to the case of χ. Unlike the case of TTF–TCNQ, where the ESR line width is *increasing* towards low temperatures, the signature of a very weak transverse coupling,[15b] the temperature dependence of the line width shown in Fig. 9b supports the existence of a spin relaxation mechanism provided by the modulation of the spin orbit coupling in a conductor far from one dimensionality. The very broad line width of 400 G in the high temperature regime (Fig. 9b) is an additional support for a strong spin–orbit interaction (probably due to the overlap of the wave-function of conduction electrons with iodine atoms), and an almost two dimensional electronic structure. Such a feature is in good agreement with the finding of a strong transverse coupling in the calculation of the electronic structure.

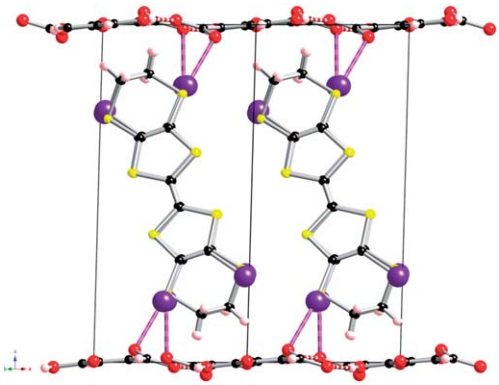

Fig. 8 The nesting vector stretches along [a*, b*], as exemplified in Fig. 7; this projection down [110] complements Fig. 5 in showing that the CDW runs exactly along the stacks in direct space.

Nevertheless the fast drop of the line width below $T = 80$ K, *e.g.* below the metal–insulator transition, provides additional evidence to the disappearance of the conduction electron susceptibility. This behavior is similar to the findings on other Q-1D metals[16] with nonmagnetic CDW ground state.

Conclusions

The primary, seminal lesson learned from this study is that the actual number of protons required within the extended fumarate network to effectively balance the chemical activity at the nuclei/solution interface during crystal growth needs not to be an integer since any amount of proton vacancies stabilized at kT is readily compensated, not by adjusting the number of components (driving the formation of polytypes or non-stoichiometric phases, for instance) but, rather, by tapping into a molecular hole reservoir, keeping the net number of molecules constant and the structure intact. A remarkable outcome is the installment of incommensurate band fillings, a very desirable prospect, as strategies for the control of the electronic band structure and

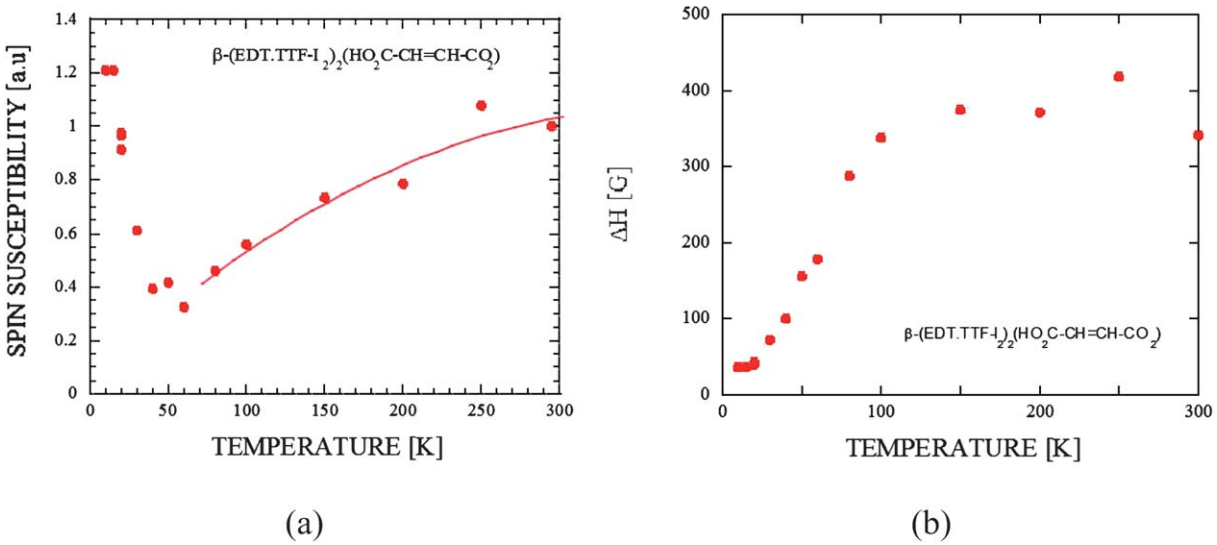

Fig. 9 a) Temperature dependence of the spin susceptibility measured by ESR. The straight line is a guide to the eye. (b) Temperature dependence of the ESR line width.

band filling by chemical means in molecular metals are much needed[17] in order to meet expectations formulated in the context of recent progress in the physics of strongly correlated systems in low dimension.[18]

Because of the particular Fermi surface topology of β-(EDT-TTF-I_2)$_2^{(1+x)\bullet+}$[HO_2C–CH=CH–CO_2^-]$_{(1-x)}$[(O_2C–CH=CH–CO_2)$^{2-}$]$_x$, there is a duality between the chemical activity and the modulus of the nesting vector which itself scales up with the net amount of proton vacancies. That is, there is a direct correlation between the chemical activity at the organic cation/organic anion interface (electrostatics) and the low dimensional physics of the system (CDW/metal–insulator transition).

A dual [proton]/[hole] mixed-valence is thereby revealed and defined as the duality between the modulation of the electrostatic potential of the environment, the incommensurate number and the physics of migrating holes within a molecular system. This unprecedented *dual* approach is currently developed further for the experimental determination of x by using the large single crystals made available (Fig. 1) to apply methodologies of low dimensional condensed matter physics, like the exploration of Fermi surface topologies by diffuse scattering[19] and magneto-resistance experiments[20] with the objective to directly deliver the amount of proton vacancies.

Acknowledgements

This work was supported by the French National Research Agency, ANR Project CHIRASYM 2005-08 (NT05-2 42710), the CNRS and the Spanish Ministerio de Educación y Ciencia (Projects FIS2009-1271-C04-03 and CSD 2007-00041). We thank the CNRS for an associated researcher position to LZ.

References

1 (*a*) P. Kathirgamanathan, S. A. Mucklejohn and D. R. Rosseinsky, *J. Chem. Soc., Chem. Commun.*, 1979, 86–87; (*b*) M. Giffard, A. Riou, G. Mabon, N. Mercier, P. Molinie and T. Phap Nguyen, *J. Mater. Chem.*, 1999, **9**, 851–853; (*c*) N. Mercier, M. Giffard, G. Pilet, M. Allain, P. Hudhomme, G. Mabon, E. Levillain, A. Gorgues and A. Riou, *J. Chem. Soc., Chem. Commun.*, 2001, 2722; (*d*) U. Geiser and J. A. Schlueter, *Chem. Rev.*, 2004, **104**, 5203–5241; (*e*) Y. Lakhdar, A. El-Ghayoury, L. Zorina, N. Mercier, M. Allain, C. Mézière, P. Auban-Senzier, P. Batail and M. Giffard, *Eur. J. Inorg. Chem.*, 2010, 3338–3342.
2 A. El-Ghayoury, C. Mézière, S. Simonov, L. Zorina, M. Cobián, E. Canadell, C. Rovira, B. Náfrádi, B. Sipos, L. Forró and P. Batail, *Chem.–Eur. J.*, 2010, DOI: 10.1002/chem.201001875.
3 (*a*) M. Armand, S. Grugeon, H. Vezin, S. Laruelle, P. Ribiere, P. Poizot and J.-M. Tarascon, *Nat. Mater.*, 2009, **8**, 120–125; (*b*) W. Walker, S. Grugeon, O. Mentre, S. Laruelle, J.-M. Tarascon and F. Wudl, *J. Am. Chem. Soc.*, 2010, **132**, 6517–6523.
4 (*a*) T. Devic, M. Evain, Y. Moëlo, E. Canadell, P. Auban-Senzier, M. Fourmigué and P. Batail, *J. Am. Chem. Soc.*, 2003, **125**, 3295–3301; (*b*) T. Devic, E. Canadell, P. Auban-Senzier and P. Batail, *J. Mater. Chem.*, 2004, **14**, 135–137; (*c*) M. Fourmigué and P. Batail, *Chem. Rev.*, 2004, **104**, 5379–5418; (*d*) A. Ranganathan, A. El-Ghayouri, C. Mézière, E. Harte, R. Clérac and P. Batail, *Chem. Commun.*, 2006, 2878–2880; (*e*) A.-L. Barrès, A. El-Ghayouri, L. V. Zorina, E. Canadell, P. Auban-Senzier and P. Batail, *Chem. Commun.*, 2008, 2194–2196.
5 P. Gilli, L. Pretto, V. Bertolasi and G. Gilli, *Acc. Chem. Res.*, 2009, **42**, 33–44.
6 Coupled electron–proton transfer issues in hydrogen-bonded TTF and TCNQ charge transfer complexes have been addressed earlier(*a*) T. Akutagawa, G. Saito, H. Yamochi, M. Kusunoki and K. Sakaguchi, *Synth. Met.*, 1995, **69**, 591; (*b*) T. Itoh, H. Kitagawa, T. Mitani and K. Nakasuji, *Chem. Lett.*, 1995, 41–42; (*c*) T. Murata, Y. Morita, Y. Yakiyama, K. Fukui, H. Yamochi, G. Saito and K. Nakasuji, *J. Am. Chem. Soc.*, 2007, **129**, 10837–10846; (*d*) J. C. Wu, N. Dupont, S.-X. Liu, A. Neels, A. Hauser and S. Decurtins, *Chem.–Asian J.*, 2009, **4**, 392–399.
7 B. Domercq, T. Devic, M. Fourmigue, P. Auban-Senzier and E. Canadell, *J. Mater. Chem.*, 2001, **11**, 1570–1575.
8 G. M. Sheldrick, *SADABS—Bruker Nonius Area Detector Scaling and Absorption Correction—V2.10*, 2003.
9 G. M. Sheldrick, *Acta Crystallogr., Sect. A: Found. Crystallogr.*, 2008, **64**, 112–122.
10 M.-H. Whangbo and R. Hoffmann, *J. Am. Chem. Soc.*, 1978, **100**, 6093–6098.
11 J. H. Ammeter, H.-B. Bürgi, J. Thibeault and R. Hoffmann, *J. Am. Chem. Soc.*, 1978, **100**, 3686–3692.
12 A. Pénicaud, K. Boubekeur, P. Batail, E. Canadell, P. Auban-Senzier and D. Jérome, *J. Am. Chem. Soc.*, 1993, **115**, 4101–4112.
13 A. L. Bednowitz and B. Post, *Acta Crystallogr.*, 1966, **21**, 566.
14 M.-H. Whangbo, J. M. Williams, P. C. W. Leung, M. A. Beno, T. J. Emge and H. H. Wang, *Inorg. Chem.*, 1985, **24**, 3500–3502.

15 (*a*) E. Canadell and M.-H. Whangbo, *Chem. Rev.*, 1991, **91**, 965–1034; (*b*) D. Jérome and H. J. Schulz, *Adv. Phys.*, 1982, **31**, 299–490.
16 (*a*) Y. Tomkiewicz and A. R. Taranko, *Phys. Rev. B: Condens. Matter Mater. Phys.*, 1978, **18**, 733; (*b*) Y. Tomkiewicz, A. R. Taranko and J. B. Torrance, *Phys. Rev. B: Solid State*, 1977, **15**, 1017.
17 (*a*) T. Mori, *Chem. Rev.*, 2004, **104**, 4947–4969; (*b*) S. Perruchas, K. Boubekeur, E. Canadell, Y. Misaki, P. Auban-Senzier, C. Pasquier and P. Batail, *J. Am. Chem. Soc.*, 2008, **130**, 3335–3348.
18 T. Giamarchi, *Chem. Rev.*, 2004, **104**, 5037–5055.
19 S. Ravy, *Chem. Rev.*, 2004, **104**, 5609–5634.
20 M. V. Kartsovnik, *Chem. Rev.*, 2004, **104**, 5737–5781.

